Silver-doped ferrimagnetic and bioactive devitrified glass for bone tumor treatment and infection prevention

Ceramics International 52 (2026) 30973–30983

Contents lists available at ScienceDirect

Ceramics International

journal homepage: www.elsevier.com/locate/ceramint

Silver-doped ferrimagnetic and bioactive devitrified glass for bone tumor treatment and infection prevention

Marta Miola [*], Matteo Bruno [1], Enrica Verné

Politecnico di Torino, Applied Science and Technology Department, Corso Duca degli Abruzzi 24, 10129, Torino, Italy

ARTICLE INFO

Keywords:
Magnetic devitrified glass
Ion-exchange
Silver
Antibacterial
Hyperthermia

ABSTRACT

Bone tumors and the resulting complications, such as the development of infections in patients immunosuppressed by conventional therapies, remain an important issue, since they can cause serious problems such as bone weakness, fractures, pain and metastases. In this work, a magnetic and antibacterial devitrified glass for bone tumor treatment and infection prevention is proposed. The magnetic devitrified glass was synthesized by the melt and quenching route, while the antibacterial effect was conferred by introducing silver through the ion exchange process, by varying silver concentration. The obtained materials were characterized from a morphological, compositional and structural point of view, evidencing the silver introduction both in metallic and ionic form. The calorimetric test evidenced the samples' ability to release heat, useful for hyperthermia treatment, when subjected to an alternating magnetic field. Finally, in vitro bioactivity tests revealed that the introduced silver did not alter the reactivity of the material, and a preliminary evaluation of the antibacterial effect demonstrated a significant inhibition zone against *S. aureus*. Therefore, the developed material exhibits promising characteristics for application in hyperthermia-based bone tumor treatment, while also providing antibacterial properties.

1. Introduction

Bone tumors, both malignant and benign, represent a critical branch of oncology since they present particular epidemiological characteristics influenced by several factors such as gender, age and genetic predispositions [1]. Although the incidence rate of bone tumors, particularly primary malignant ones, is not very high (0.2% of all malignancies), the overall survival rate is low, while recurrences are significant [2]. The treatments currently used for bone tumors include surgery, supported by chemotherapy and/or radiotherapy. However, surgery often fails to completely eradicate the tumor, resulting in metastases and recurrence. Radiotherapy and chemotherapy have several side effects, such as bone death or osteoradionecrosis, cardiotoxicity, liver damage, and suppression of bone marrow [3].

In addition to conventional therapies, several treatments are currently being investigated in both preclinical studies and the literature, such as immunotherapy, targeted therapy and gene therapy. Among these, biomaterial-based strategies are attracting considerable interest because they can combine therapy with bone support and regeneration [4,5]. Magnetic materials are deeply investigated because they can generate localized heat when exposed to an external alternating magnetic field and can therefore be used for hyperthermia treatments [6,7]. Magnetic materials for hyperthermia include iron oxides, ferrites, and metal alloys [6,8]. Magnetic devitrified glasses, particularly bioactive ones, have attracted the attention of researchers for their potential to destroy tumor cells and, at the same time, stimulate osseointegration [9–14].

A serious complication associated with bone tumor surgery is the development of infections [15,16], particularly in patients immunosuppressed by conventional therapies. To solve this issue, magnetic materials with antibacterial properties have been proposed [17]. Some authors have developed composite materials containing a magnetic and an antibacterial phase; for example, Hlukhaniuk et al. [18] proposed bifunctional PCL scaffolds containing magnetic nanoparticles and tannic acid as an antibacterial agent. Other research works combined the magnetic hyperthermia and the release of antineoplastic agents [19–21].

Silver has long been studied to impart antimicrobial properties to

* Corresponding author. Politecnico di Torino, Department of Applied Science and Technology (DISAT), Corso Duca degli Abruzzi 24, 10129, Torino, Italy.
E-mail address: marta.miola@polito.it (M. Miola).
[1] Present affiliation: DIPROMED srl. Via Ciriè 22, 10099 San Mauro Torinese, Torino, Italy.

https://doi.org/10.1016/j.ceramint.2026.05.156
Received 12 January 2026; Received in revised form 27 April 2026; Accepted 11 May 2026
Available online 12 May 2026

bioactive glasses and glass-ceramics [22–25]. Silver can be introduced as a reagent into glass precursors synthesized via casting and melting or sol-gel process, or it can be introduced through ion exchange technique. Its introduction does not affect the bioactivity of the glass; on the contrary It has been highlighted that it participates in the bioactivity process with the same role as sodium [26]. However, its content must obviously be carefully calibrated to avoid toxic effects [24,27]. The incorporation of metal ions with antibacterial properties into bioactive magnetic glass or glass ceramic materials is still little investigated in the literature. For example, the work of Sharma et al. [28] reports the synthesis of magnetic glass ceramics containing up to 4 mol% silver via a melt quenching process. The resulting material exhibits good antibacterial activity but is not bioactive.

Recently, the authors proposed the introduction of silver and copper in a bioactive and magnetic devitrified glass composition to obtain a multifunctional material [29–31]. The introduction of the two antibacterial elements as starting reactants during the materials production by the melt and quenching process did not lead to good results in terms of antibacterial properties; furthermore, the used technique for Cu introduction strongly influenced the formation of magnetite, with consequent decrease in the capacity to release heat [30]. The introduction of copper using the ion exchange technique did not affect the heating capacity of the material; however, the antibacterial properties could still be improved [31].

In this work, the introduction via ion exchange of silver as an antibacterial agent in a magnetic devitrified glass composition for the treatment of tumors in hyperthermia and the prevention of infections was evaluated. The material was characterized in terms of morphology, composition, heating ability, bioactivity and preliminary antibacterial properties. The obtained results highlight the efficacy of the adopted technique to synthesize a multifunctional material for the treatment of bone tumors.

2. Materials and methods

2.1. Synthesis of the bioactive devitrified glass

The material object of the present work (SC45) is a silica-based partially devitrified glass with the following composition (wt%): 24.7% SiO_2, 13.5% CaO, 13.5% Na_2O, 3.3% P_2O_5, 31% Fe_2O_3, 14% FeO. It was obtained by the addition of Fe_2O_3 and FeO to the composition of the bioactive glass 45S5 (Bioglass®) in proportions chosen to induce, during casting of the melt, the crystallization of magnetite (ideally the theoretical value of 45 wt%) as the only one crystalline phase inside the residual amorphous phase, to assure both ferrimagnetic behavior (thus, heat capacity generation) and bioactivity of the material [32–34]. High purity raw materials were used: Na_2CO_3 (Sigma-Aldrich, ≥99,5%), $CaCO_3$ (Sigma-Aldrich, ≥99%), SiO_2 (Sigma-Aldrich ≥99%), $Ca_3(PO_4)_2$ (Fluka ≥96%), $FeSO_4$*$7H_2O$ (Sigma-Aldrich, ≥99%) and Fe_2O_3 (Sigma-Aldrich ≥99%). The powder precursors were automatically mixed on a mixing roller for 15 min. The reactants were then heated in a platinum crucible up to 1550 °C, using a heating rate of 10 °C/min, inside a high temperature furnace (Nabertherm - Carbolite 1800) and maintained in temperature for 25 min, up to complete melting. The melt was then cooled at room temperature in air by pouring it into a brass mold. During cooling, a partial devitrification of the amorphous phase occurred, resulting in a high conversion of iron oxide into magnetite crystals in the bulk samples. The bulk was then milled with a Planetary Ball Mill (Vibratory Micro Mill PULVERISETTE 0 Fritsch) in a zirconia jar. The milled powders were then sieved below 20 μm.

The ion exchange process was applied to the SC45 powders, aiming to introduce Ag^+ ions in substitution of Na^+ ones. The ion exchange, as already described in Ref. [34] involves the exchange of alkali ions between a molten salt and a glass surface, followed by the interdiffusion of ions into the glass. The reaction 1) clarifies the ion exchange process:

Table 1
Different molar concentrations of the salts used for ion exchange and sample identification of SC45.

Sample identification	$NaNO_3/AgNO_3$ mol/mol	Silver content
SC45-Ag 20	20	High
SC45-Ag 200	200	Medium
SC45-Ag 2000	2000	Low

$$Na^+_{(glass)} + Ag^+_{(molten\ salt)} \rightarrow Ag^+_{(glass)} + Na^+_{(molten\ salt)} \quad 1)$$

A thin layer of SC45 particles was interposed between two layers of previously mixed salts, sodium nitrate ($NaNO_3$, Sigma Aldrich, melting temperature = 310 °C) and silver nitrate ($AgNO_3$, Sigma Aldrich, melting temperature = 210 °C), inside a silica crucible (purity >99%). The crucible was introduced into an alumina cup and placed into an oven (Manfredi-1200 °C). The ion exchange treatment was performed for 30 min at 380 °C, with a heating rate of 10 °C/min. After the thermal treatment, the crucible was removed from the oven and the melt was quenched on a brass plate. Three washing treatments in distilled water at room temperature were performed in ultrasound equipment to remove residual salts, favoring the dissolution of the salts and the separation of SC45 powders. At the end of the washing treatments, residual water was removed and the SC45 powders were filtered and dried in an oven at 60 °C overnight. Three ion exchange conditions were investigated for different Na/Ag molar ratios (20, 200, 2000) to study the effect of silver molar concentration on SC45 properties. Table 1 summarizes the ion exchange conditions and the corresponding sample identification.

2.2. Characterization

2.2.1. Morphological, compositional and phase analysis

The morphology and composition of SC45 and Ag-doped SC45 powders were investigated by means of field emission electron microscopy (FESEM – SUPRATM 40, Zeiss) equipped with energy dispersion spectrometry (EDAX PV 9900) after chromium-coating of the samples.

The structure of SC45 before and after silver doping was investigated by X-Ray diffraction (X'Pert Philips diffractometer), using the Bragg Brentano camera geometry with Cu-Kα incident radiation, source voltage and current set at 40 kV and 30 mA, step size $\Delta(2\theta) = 0.02°$, fixed counting time of 1 s per step. The spectra were acquired and analyzed with the "X'Pert High Score" program, comparing the experimental data with the PCPDFWIN database (2002 JCPDS- International Centre for Diffraction Data) and quantifying the amount of crystalline phases by using the Reference Intensity Ratio (RIR) method in Panalytical's X'Pert HighScore Plus software.

2.2.2. Calorimetric test

A calorimetric test was performed on SC45 samples using an alternate magnetic field with the aim of detecting the increase in temperature of a known volume of water containing samples of defined size, weight and morphology. The test was developed using a magnetic induction furnace Egma 6 (Felmi S.r.l), generating a magnetic field intensity of 22.5 mT at fixed working frequency of 220 kHz. 0.5 g of powder samples were immersed in 16 ml of distilled water and the initial temperature (T_{in}) was measured with a thermocouple. Then, the tube containing the samples was positioned in the middle of the coils of the inductor and covered with a polyethylene foam thermal insulator to reduce heat dispersion. The convective motion of the water inside the test tube induced particle movement. A magnetic induction was applied and the final temperature (T_{fin}) was measured after 2, 4, 6 and 8 min. After each measurement, samples were cooled in air at room temperature. The same test was repeated three times for each powder formulation to minimize the data scattering.

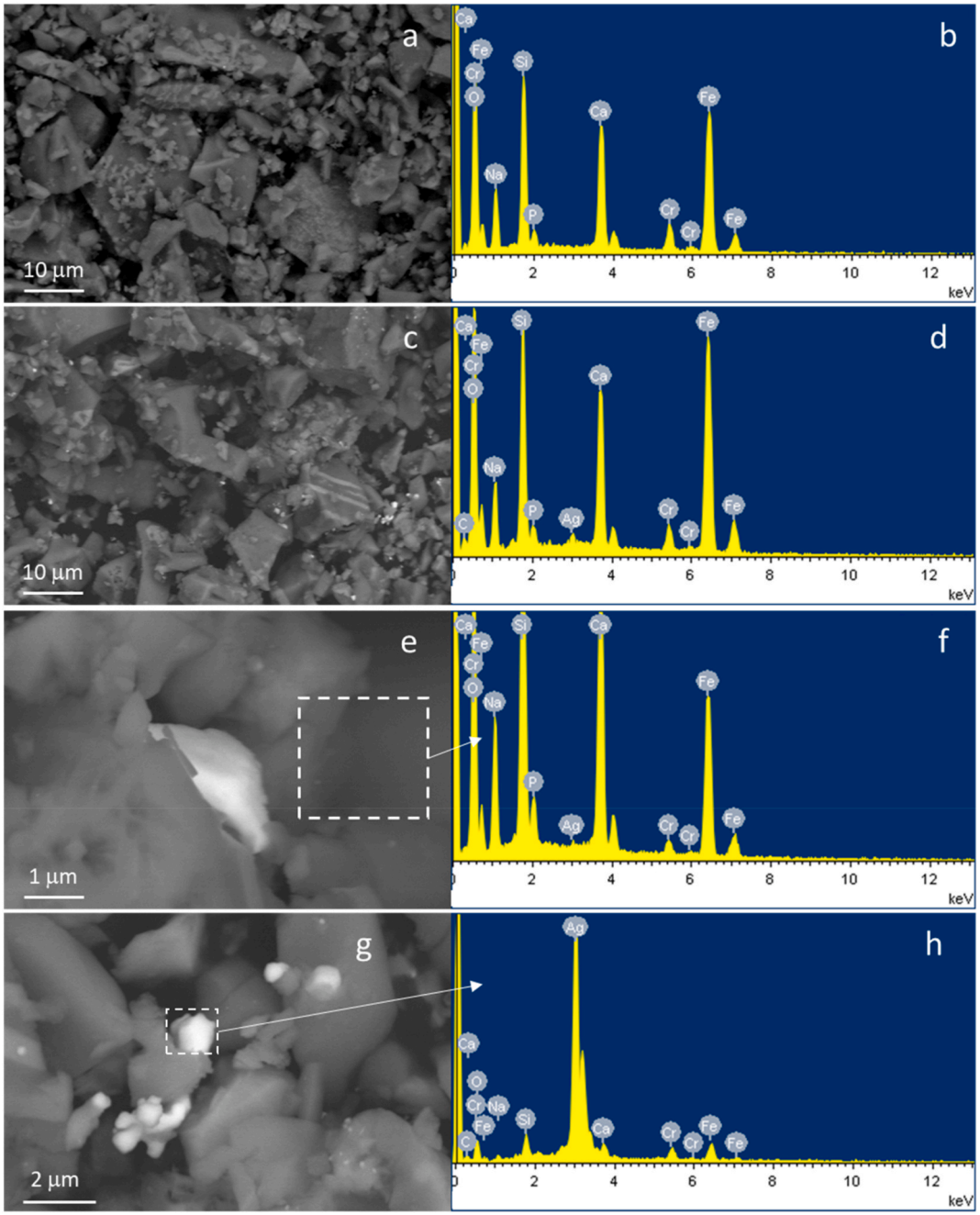

Fig. 1. FESEM-EDS analysis of SC45 (a,b) and SC45-Ag2000 (c-h).

2.2.3. Bioactivity tests

Bioactivity test was performed on SC45 samples doped with silver, compared with the control (SC45), by immersion in simulated body fluid (SBF) up to 4 weeks [35]. 100 mg of powder was soaked in 100 ml of SBF and stirred in an orbital shaker (150 rpm), at the temperature of 37 °C. The refresh of the solution was not performed to avoid particle loss. The pH of the SBF was monitored every two days by using a digital pH meter. After three and four weeks, powders were removed from the solution by filtering, dehydrated in an incubator for one day at 37 °C and analyzed using FESEM-EDS.

2.2.4. Antibacterial properties

The antibacterial properties of the samples were investigated by the inhibition halo test, according to the National Committee for Clinical Laboratory Standards (NCCLS) [36], using a *Staphylococcus aureus* standard strain (ATCC 29213). The samples were produced using 200 mg of SC45 and silver-doped SC45 powders, uniaxially pressed at 4 tons for 10 s in order to prepare pellets of a diameter of 1 cm and a thickness of 0,5 mm. The pellets were placed on a Mueller Hinton agar plate, uniformly covered with a previously prepared bacterial broth [37], and incubated overnight at 35 °C. After 24 h, the results were evaluated by observing and measuring the halo of inhibition formed around the samples, which indicates the non-proliferation of bacteria.

3. Results and discussion

3.1. Morphological, compositional and phase analysis

Morphological and compositional analyses of Ag-doped SC45 powders, both on a wide area and on specific particles, were performed and

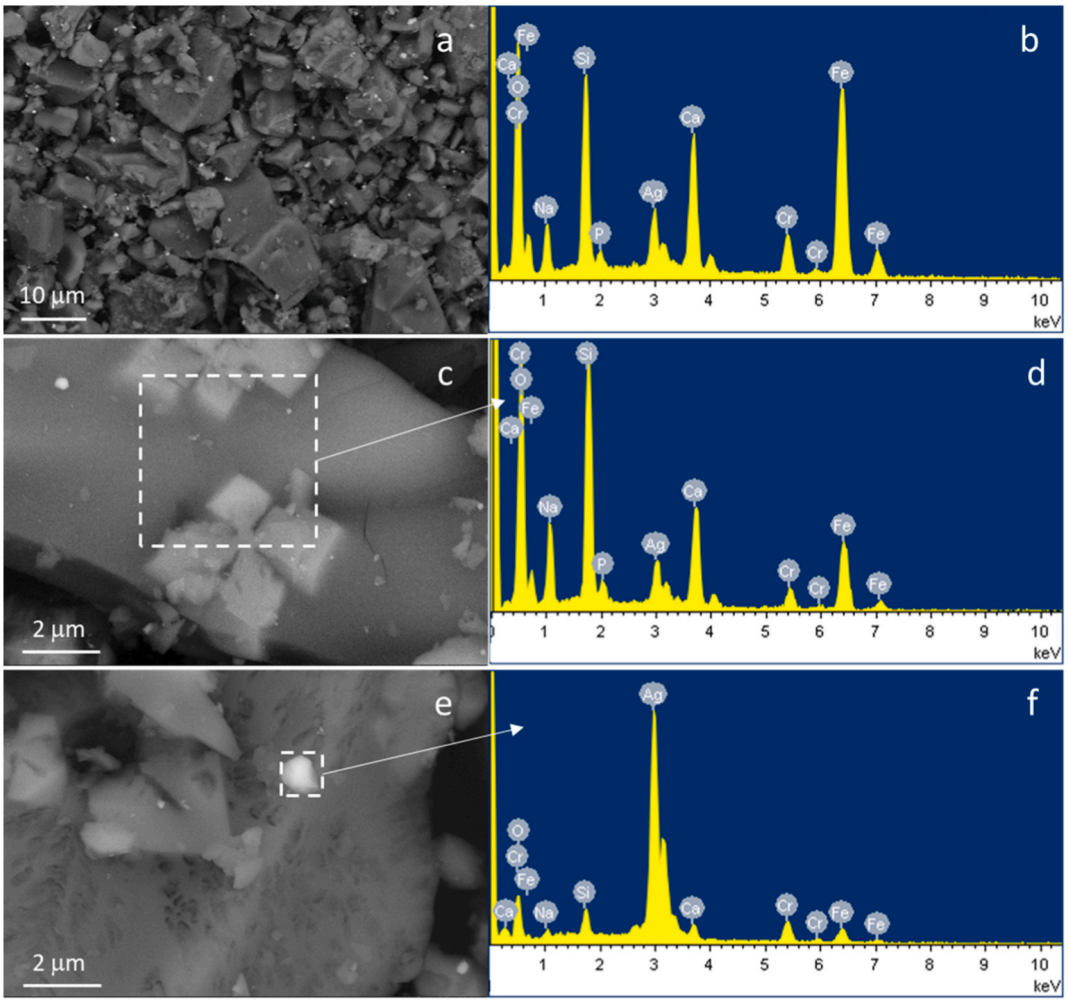

Fig. 2. FESEM-EDS analysis of SC45-Ag200.

reported below. Fig. 1(a and b) also reports for comparison a micrograph of SC45 powders and related compositional analysis.

Fig. 1c reports a backscattering image area of SC45 particles <20 µm after the ion exchange in molten salt with low silver conditions (SC45-Ag2000), white arrows evidence the different brightness of precipitates that are attributed to a silver-rich phase. Fig. 1d reports the EDS area analysis that shows the presence of silver and chromium (the last one comes from the metallization of the sample). Silicon, calcium, phosphorus, iron and oxygen are typical of the SC45 composition, while silver is introduced during the molten salt ion exchange procedure.

Fig. 1e and g shows in more detail some SC45-Ag2000 powders in backscattering at higher magnification. The presence of bright silver-rich particles is clearly evident, as confirmed by the EDS analysis performed on one of them, where the peak of silver is the highest of the spectra (Fig. 1h). Ag particles have a submicron size or just over a micron and they are not completely embedded into the glass matrix. Fig. 1 e and f reports a morphological and compositional analysis performed on a wide area of a SC45-Ag2000 particle. As it can be seen from the EDS, the peak of silver is lower with respect to the other atomic elements. Probably, in this area, silver ions entered into the glass matrix without the formation of micrometric precipitate.

Fig. 2a reports the morphology of particles of SC45-Ag200; it is possible to observe a large number of light spots, as evidenced by the arrows, which can be attributed to silver-rich precipitates. The area EDS (Fig. 2b) shows a higher peak of Ag than the SC45-Ag2000 sample. While Fig. 2e reports a morphological analysis of a SC45-Ag200 particle in which it is possible to distinguish a precipitate on the SC45 matrix, as evidenced by the EDS in Fig. 2f (performed on the precipitate), which highlights a peak of silver very sharp and high respect to the peaks of glass elements.

Fig. 2c and d reports morphological and compositional analysis in an area of the sample without precipitates, where the peak of silver is still clearly visible. It could be assessed that in this area, silver has been introduced in the glass-ceramic matrix, probably in ionic form, by ion exchange. Moreover, a columnar crystal of magnetite of about 3 µm embedded into the SC45 matrix is also observable.

Finally, Fig. 3 reports the morphology and the composition of the SC45-Ag20 sample. Also in this case, some bright spots are well visible in the image of area (Fig. 3a) and the area EDS confirms the presence of a very high silver amount (Fig. 3b) together with the other chemical components of SC45.

Fig. 3c and e report a magnification of SC45-Ag20 particles. Silver seems to be entered in the vitreous network as confirmed by EDS in Fig. 3d and, as in the other samples, precipitated as silver-rich phase as confirmed by the EDS analysis performed on a bright precipitate, which evidences a strong peak of Ag (Fig. 3e and f).

Table 2 resumes the semiquantitative analysis performed on top of doped and undoped SC45 samples.

The sample SC45-Ag2000 shows a decrease of Na content of 3 % respect to the undoped SC45 and a presence of Ag in atomic percentage of 0,73%. This agrees with the ion exchange mechanism, since the sodium ions come out from the glass network (as modifier ions) and are replaced by silver ions, which are present in the molten salt bath. In this case, sodium ions are not completely replaced by silver ones.

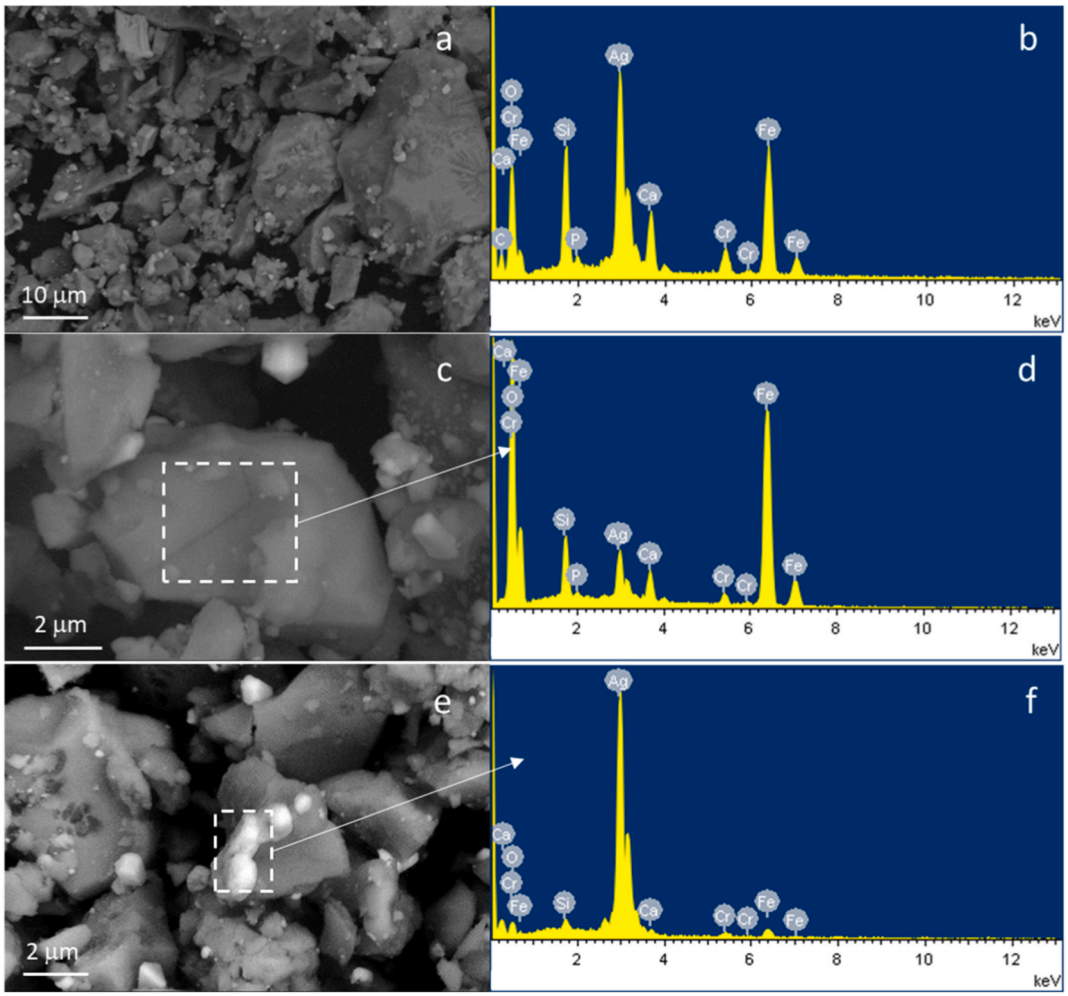

Fig. 3. FESEM-EDS analysis of SC45-Ag20.

Table 2
EDS analysis (at%) on doped and undoped SC45 samples, average values and standard deviations.

	SC45	SC45-Ag2000	SC45-Ag200	SC45-Ag20
Na	22.5 ± 0.1	19.5 ± 0.9	16.3 ± 0.1	1.8 ± 0.2
Si	21.3 ± 0.2	22.1 ± 0.8	20.8 ± 0.5	20.4 ± 0.4
P	1.6 ± 0.1	1.7 ± 0.1	1.3 ± 0.09	1.4 ± 0.2
Cs	16.5 ± 0.1	14 ± 0.1	14.8 ± 0.3	12.3 ± 0.4
Fe	38 ± 0.1	42 ± 1.5	41.4 ± 0.8	40.5 ± 0.8
Ag	/	0.7 ± 0.0	5.4 ± 0.2	23.5 ± 0.6

The atomic percentage of sodium decreases and is substituted by silver, also in the sample SC45-Ag200. The introduced silver amount is greater than SC45-Ag2000. Silicon and phosphorus remain constant, in the same way calcium decreases due to the effect of the ion exchange process, while iron remains stable.

The EDS analysis related to SC45-Ag20 evidences a very high depletion of sodium and a clear decrease of calcium, a slight increase of iron and the introduction of 23.5 at% of silver into the glass-ceramic. The ionic exchange involved mainly sodium and silver. This depends on whether silver ions possess an atomic ratio similar to sodium.

Fig. 4 reports the XRD pattern of Ag-doped SC45 samples and pristine SC45 as a control. As previously observed by the authors [29,30], the SC45 pattern shows magnetite (ref. 01-075-1609, 99%) as the main crystalline phase, along with a very weak signal of hematite at 33,2° (ref. 00-013-0534, 1%). A similar result was observed by Sharma et al. in a work concerning the synthesis of a magnetic glass-ceramics [28], even if with a different composition. The pattern of SC45-Ag2000 is very similar to the pristine SC45, showing magnetite as the main crystalline phase (79%), a more intense signal of hematite (19%) and also metallic silver (ref. 01-089-3722, 2%). Even SC45-Ag200 pattern shows magnetite as the main crystalline phase (78%), together with metallic silver peaks (5%) and a signal of hematite, comparable with SC45-Ag2000 (17%). The X-ray analysis performed on SC45-Ag20 shows again magnetite as the main crystal phase (59%) and very intense and narrow peaks of metallic silver (17%). Hematite are always present (24%), and it is remarkable that this phase was detected in increasing intensity as the signals of metallic silver increased. At low diffraction angles between 20 and 35°, a halo typical of an amorphous phase is also detected.

A hypothesis on the chemical transformation observed on all SC45 doped samples with three different molar concentrations of silver nitrate could be the possibility of a redox reaction between iron and silver on samples surface. As already noted by the authors in another work, it can be hypothesized that the reduction of Ag^{+} to Ag° could be promoted by the partial oxidation of Fe_3O_4 to Fe_2O_3 [29]. From a theoretical point of view, silver ions in an aqueous solution tend to reduce with the following reaction:

$$Ag^{+}(aq) + e^{-} \Longrightarrow Ag(s) \quad (1)$$

Silver has a higher reduction potential than iron [38], so it is more inclined to reach a stable metallic form with a consequent oxidation of iron. The chemical reaction developed is:

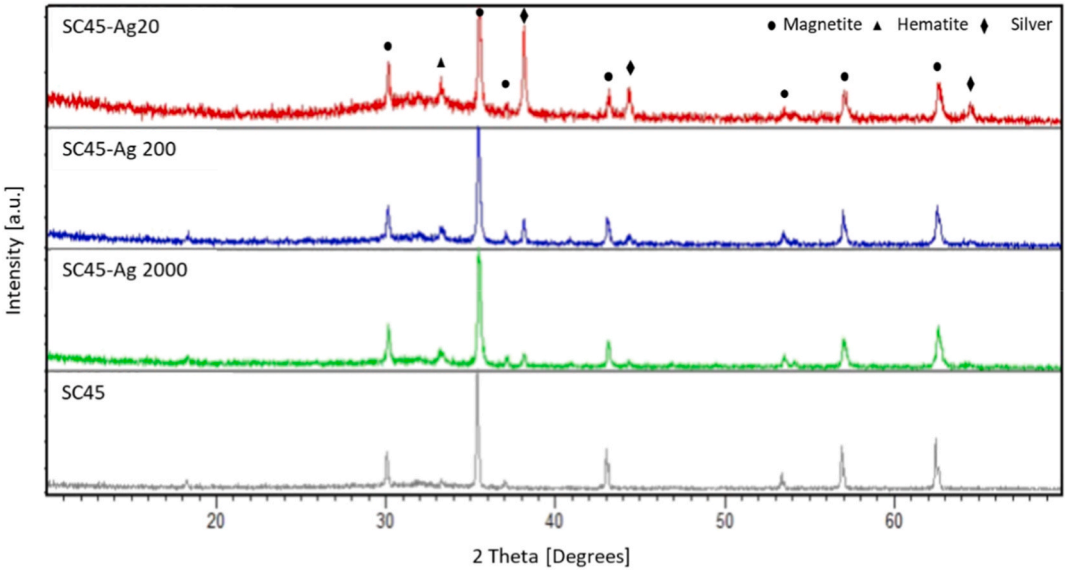

Fig. 4. X ray diffraction patterns of SC45 and Ag-doped SC45.

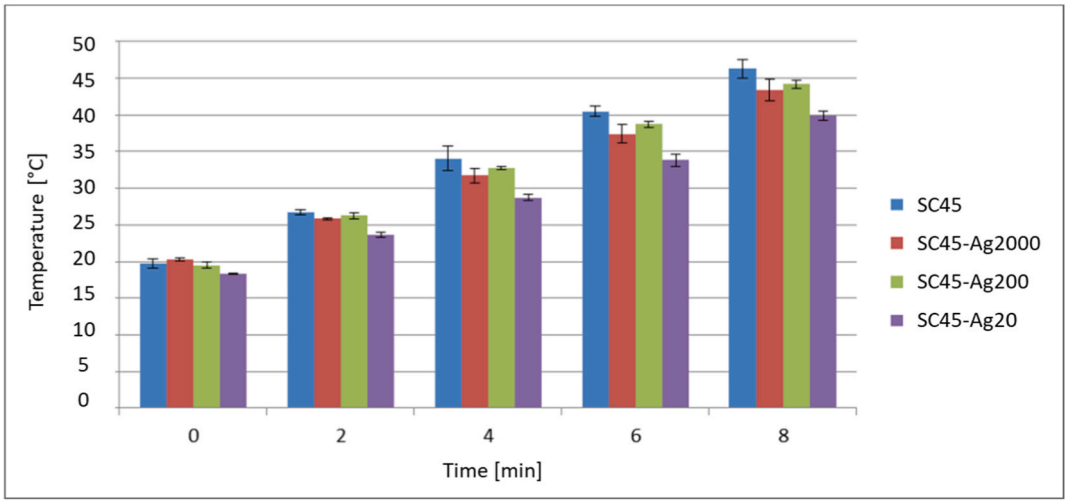

Fig. 5. Calorimetric test on pristine SC45 and SC45 doped with silver.

$$Fe^{2+} + Ag^{+} \rightarrow Fe^{3+} + Ag \quad (2)$$

Increasing the concentration of silver nitrate in the molten salt leads to a greater formation of metallic precipitates. According to reaction (2), the appearance of metallic silver precipitates may also be linked to the oxidation of Fe^{2+} ions and, consequently, to the partial conversion of magnetite into hematite.

From these results, it is reasonable that silver has been introduced in two different chemical forms: as metallic particles, confirmed by XRD and morphological analysis, and as ionic specie, as verified by compositional analysis.

3.2. Calorimetric measurement

Fig. 5 shows the temperatures reached by the powders of SC45, doped and undoped with silver, during the calorimetric test. The temperature of SC45 always increases a little more than all silver-doped samples. SC45-Ag2000 and SC45-Ag200 have similar behavior and they maintain their temperature a few degrees (°C) below the control, while SC45-Ag20 sample presents a slight decrease in heating at all time points compared to the other samples. The observed slight decrease is partially attributable to surface oxidation of Fe_3O_4 to Fe_2O_3, as well as to the reduced fraction of the magnetic phase associated with the incorporation of silver nanoparticles, for the same sample mass. Overall, the introduction of silver neither improves nor significantly degrades the heat-generation capability. Indeed, after 8 min, the average temperature recorded, on three repeated tests, is reported to be between 40 °C and 45 °C. This confirms the possibility of the hyperthermia application for all the magnetic materials objects of the present investigation.

The above-mentioned results are consistent with those reported by the authors in a previous study [29], in which silver oxide was introduced as a reagent during the synthesis of SC45 glass through a melting–quenching process. In that work, the nucleation of metallic silver nanoparticles within the bulk was observed, occurring according to reaction (2). Accordingly, more intense hematite signals were detected in the XRD patterns. In that system, metallic silver also promoted the nucleation and growth of magnetite crystals, exerting a slight influence on the magnetic properties, while not affecting the heating capability of the silver-doped samples. This nucleation effect is not observed in the present study, as silver is introduced by ion exchange at the surface of an already devitrified glass.

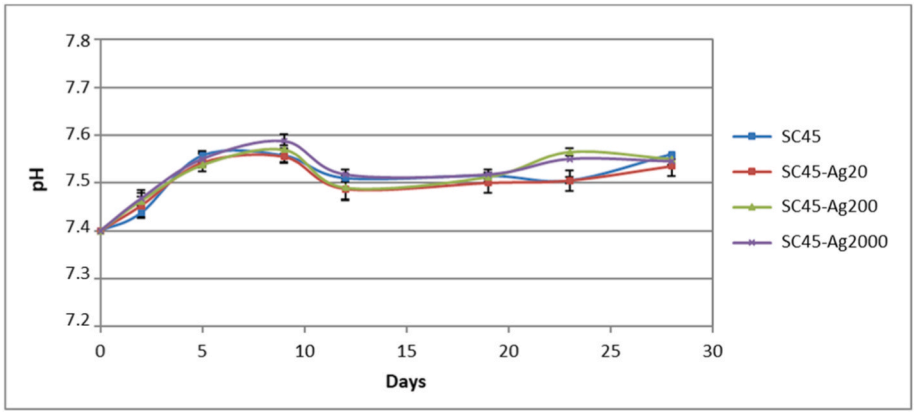

Fig. 6. pH variation of the SBA solution containing the samples doped with Ag and the SC45 control.

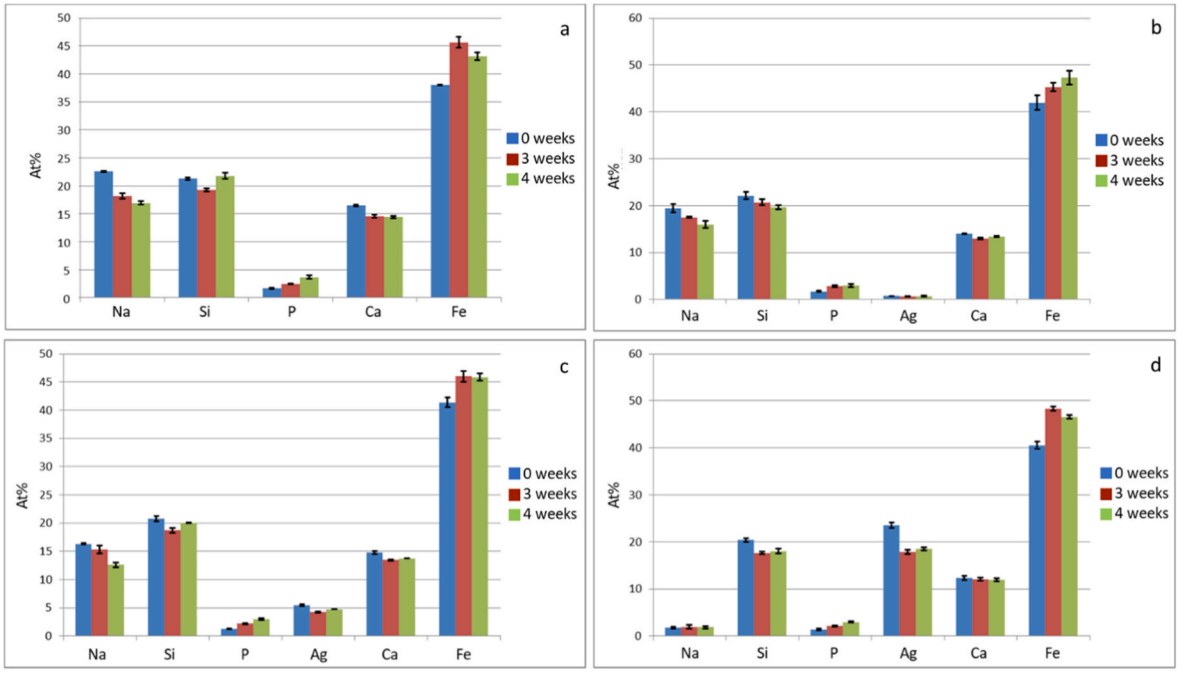

Fig. 7. EDS analysis of a) SC45, b) SC45-Ag2000, c) SC45-Ag200 and d) SC45-Ag20.

3.3. Bioactivity tests

To evaluate the result of the bioactivity test, the trends of the solutions pH, containing samples of different compositions, have been compared. To verify the reactivity in SBF and the possible nucleation of silica gel or hydroxyapatite precursors, the samples were analyzed using SEM and EDS analyses.

Any significant variation in the pH value during the test can be noticed among the different compositions of silver-doped glass-ceramic, if compared to the control (SC45). The pH was almost stationary and oscillated between 7.4 (starting value, physiological pH) and 7.65 (Fig. 6). The recorded values fluctuate within the range considered acceptable by human cells (7.0-7.8).

The reactivity of SC45 during soaking in SBF was also assessed by evaluating the percentage of surface concentration of the elements potentially involved in the bioactivity process, comparing the trend of sodium, silicon, phosphorus, calcium, silver and iron before the treatment (0 weeks), after 3 and 4 weeks in SBF. The obtained results are reported in Fig. 7.

Concerning SC45 (Fig. 7a), it can be observed that sodium decreases both after three and four weeks in SBF, silicon is slightly reduced after three weeks and then returns to a value close to the starting point, phosphorus increases in time, calcium is slightly reduced but it is stable at three and four weeks, while iron increases after three weeks, then slightly decreases at four. This trend is in agreement with the bioactivity process: sodium is typically released in SBF solution and replaced with H_3O^+ ions and silicon increases at 4 weeks due to the presence of silica gel formation. The phosphorus' increase is justifiable according to the process of bioactivity, which provides precipitation of phosphates on the surface of the sample. The EDS analysis of area shows more iron in the exposed glass particles at 3 weeks because the development of ionic exchange-glass solution has partially dissolved the glassy matrix. The reduction at 4 weeks can be related to the formation of a phosphate-rich silica gel layer that partially covered the magnetite particles previously exposed.

The trend of the elements for the samples containing Ag (Fig. 7b,c and d) does not significantly differ from what was observed for the control sample. In particular, it can always be noticed an increase in P and a decrease in Na, except for the SC45-Ag 20 sample, in which the decrease in Na is hardly detectable due to its low content following the

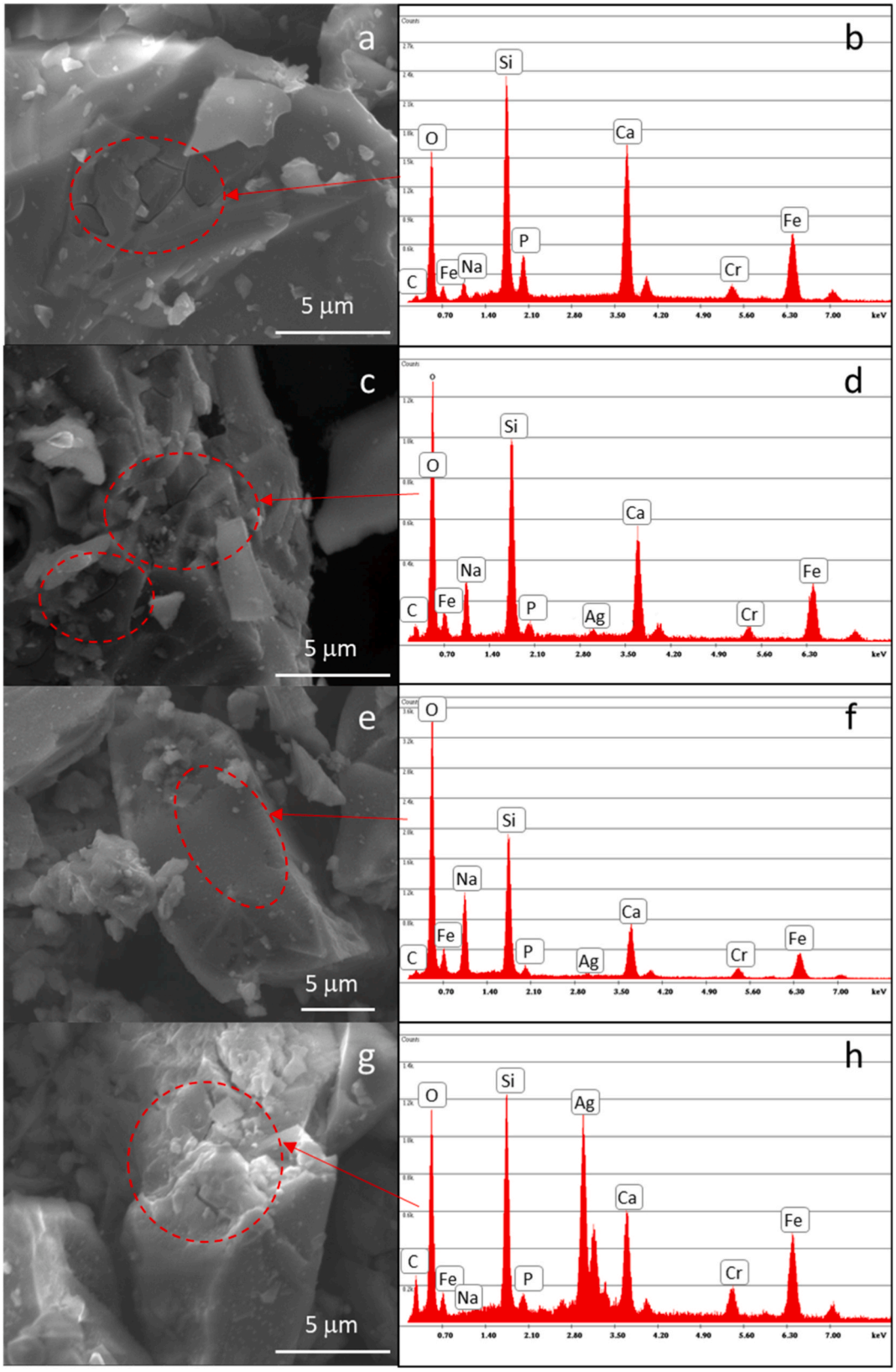

Fig. 8. SEM micrographs and EDS analyses of SC45 (a, b), SC45- Ag 2000 (c, d), SC45 Ag 200 (e, f) and SC45- Ag 20 (g, h) after 3 weeks of immersion in SBF solution.

ion exchange with Ag. However, it was verified that silver ions can participate in the bioactivity process with the same role as sodium [26]. When they are released, the non-bridging oxygen atoms create the conditions for silica gel formation, which will subsequently evolve into hydroxyapatite [39].

Fig. 8 reports a morphological and compositional analysis of SC45 undoped and doped with silver, after 3 weeks in SBF. The results do not indicate the presence of apatite, but rather a flat surface composed of

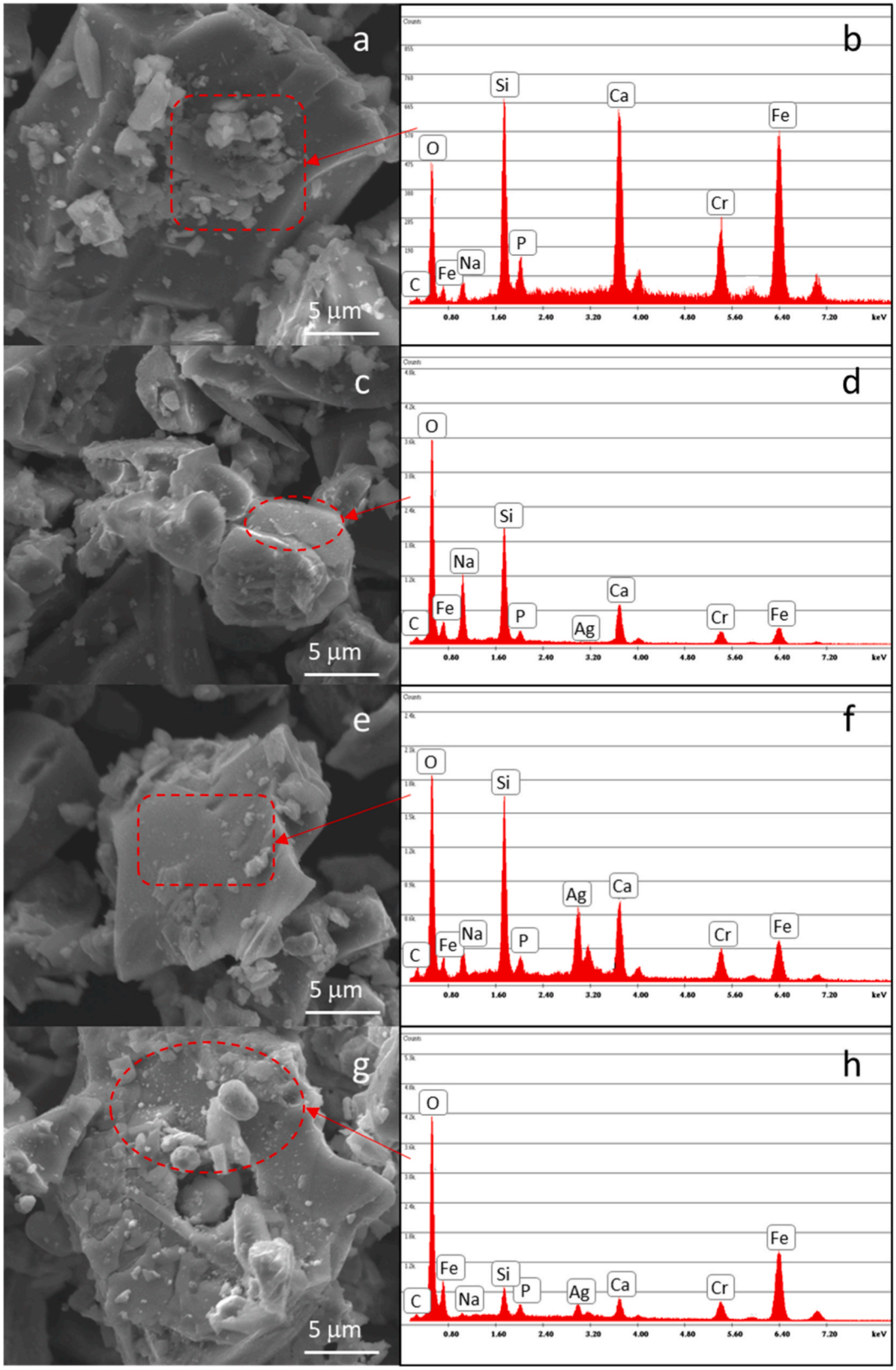

Fig. 9. SEM micrographs and EDS analyses of SC45 (a, b), SC45- Ag 2000 (c, d), SC45- Ag 200 (e, f) and SC45- Ag 20 (g, h) after 4 weeks of immersion in SBF solution.

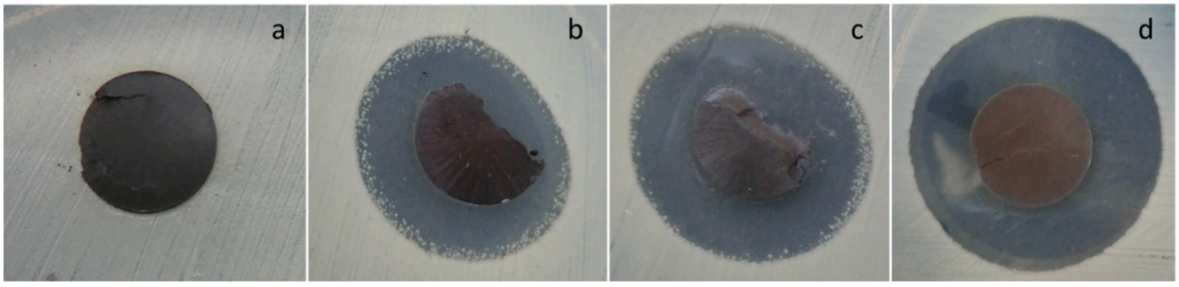

Fig. 10. Inhibition halo test of a) SC45, b) SC45-Ag2000, c) SC45-Ag200 and d) SC45-Ag20.

Table 3
Mean value of the inhibition halo diameter.

Sample	Inhibition halo diameter [mm]
SC45	0
SC45-Ag2000	5
SC45-Ag200	5,7
SC45-Ag20	6,7

silica enriched in Ca and P, as confirmed by local EDS analysis, which shows high peaks of silicon, along with calcium and phosphorus. The cracks observed in the pictures (evidenced with dotted red circles) are a common morphological feature for silica-gel grown on bioactive material.

Fig. 9 reports the morphology and compositional analysis of undoped and Ag-doped SC45 particles after 4 weeks of soaking in SBF. As in the previous case, the precipitates with the typical morphology of hydroxyapatite were not observed; however, Si, Ca and P rich areas were noticed, highlighting a certain degree of reactivity of the material. As observed in previous works [33], the bioactivity kinetics of SC45 are slow; however, the presence of silver does not seem to have interfered with the bioactivity mechanism, since, as previously underlined [26], silver plays the same role as sodium in the bioactivity process. Indeed, other works evidenced a maintained or even enhanced bioactivity for silver-doped bioactive glasses [25,40], highlighting that the incorporation of silver is fully compatible with the mechanisms governing bioactivity.

3.4. Antibacterial properties

Fig. 10 shows the results of the inhibition halo test performed on Ag-doped and undoped SC45 samples. All samples containing Ag produced a significant inhibition halo between 5 and 6.7 mm. SC45-Ag2000 and SC45-Ag200 samples show the presence of a double halo: a first well-defined halo in direct contact with the sample surface and a second one (more peripheral) in which some colonies begin to proliferate. On the contrary, SC45-Ag20 sample produced a uniform halo. In fact, the silver concentration decreases away from the sample until reaching, for Ag 200 and 2000, a value for which some bacterial colonies begin to survive and proliferate. With respect to the melting and quenching techniques previously investigated by the authors [22], the SC45 doped with silver by ion exchange in molten salts produced a very wide antibacterial effect due to the preponderance of ionic form and metallic particles.

Table 3 reports the mean values of the inhibition halo produced by SC45 samples undoped and doped with silver. As expected, increasing the silver concentration the diameter of the halo increases. The antibacterial effect obtained for these samples indicates a contribution of both the silver ions present in the glassy network and the nanometric precipitates that were observed in all three formulations by FESEM-EDS and XRD. In fact, even if the concentrations of silver in the samples are very different from each other, all of them produced very wide and sharp halos; this indicates that a large contribution to the antibacterial effect was given by silver present in all samples in its different forms. For example, SC45-Ag 2000 does not contain a particularly high amount of silver within the glass network; however, it exhibits several precipitates of metallic silver, which contribute to the formation of the halo.

4. Conclusions

Three different molar concentrations were used to prepare a silica-based devitrified glass containing magnetite (SC45) doped with silver (SC45Ag2000, SC45Ag200, SC45Ag20). The morphological and compositional analysis evidenced on all samples the presence of silver sub-micrometric metallic precipitates in different amounts, as well as the presence of ionic silver in the amorphous matrix.

X-ray diffraction investigations confirmed the presence of metallic silver in all samples. No additional crystalline phases were detected, apart from magnetite and, in some cases, traces of hematite, whose intensity increases with the increasing amount of metallic silver. The calorimetric measurements presented a linear increasing trend with time for all samples. A slight decrease relative to the control was observed only for SC45Ag2000.

Bioactivity characterization was performed on the samples after three and four weeks of soaking in SBF. The reaction kinetics of these materials were relatively slow, and even after four weeks of treatment, no crystalline hydroxyapatite was detected on the sample surfaces; only a thin silica gel layer was observed. However, the introduction of silver did not affect the reactivity of the material. The presence of a thin silica gel layer was detected in several samples. This result was confirmed by compositional analysis, which revealed a local increase in phosphorus compared with the control sample, although no structural modification of the surface was observed. Encouraging results came even from the antibacterial characterization for all silver-doped samples, which presented a wide inhibition zone, where no bacteria grew and proliferated, highlighting a contribution of silver in both metallic and ionic form.

Since the formation of metallic silver particles could partially affect the reproducibility of the synthesis outcome, future studies should investigate the optimization of process parameters (temperature, salt concentration, and time) and the use of treatments under controlled atmosphere to achieve improved control of the redox chemistry between iron and silver ions.

CRediT authorship contribution statement

Marta Miola: Writing – review & editing, Writing – original draft, Visualization, Methodology, Investigation, Conceptualization. **Matteo Bruno:** Writing – original draft, Validation, Investigation, Formal analysis. **Enrica Verné:** Writing – review & editing, Writing – original draft, Supervision, Resources, Project administration, Conceptualization.

Declaration of competing interest

The authors declare that they have no known competing financial interests or personal relationships that could have appeared to influence the work reported in this paper.

References

[1] H. Hosseini, S. Heydari, K. Hushmandi, S. Daneshi, R. Raesi, Bone tumors: a systematic review of prevalence, risk determinants, and survival patterns, BMC Cancer 25 (1) (2025) 321, https://doi.org/10.1186/s12885-025-13720-0.

[2] J. Lai, X. Li, W. Liu, Q. Liufu, C. Zhong, Global, regional, and national burden and trends analysis of malignant neoplasm of bone and articular cartilage from 1990 to 2021: a systematic analysis for the global burden of disease study 2021, Bone 188 (2024) 117212, https://doi.org/10.1016/j.bone.2024.117212.

[3] R. Shao, Y. Wang, L. Li, Y. Dong, J. Zhao, W. Liang, Bone tumors effective therapy through functionalized hydrogels: current developments and future expectations, Drug Deliv. 29 (1) (2022) 1631–1647, https://doi.org/10.1080/10717544.2022.2075983. Dec.

[4] J. Liao, R. Han, Y. Wu, Z. Qian, Review of a new bone tumor therapy strategy based on bifunctional biomaterials, Bone Res. 9 (2021) 18, https://doi.org/10.1038/s41413-021-00139-z.

[5] Y. Zhang, Y. Wu, X. Qiao, T. Lin, Y. Wang, M. Wang, Biomaterial-based strategy for bone tumor therapy and bone defect regeneration: an innovative application option, Front. Mater., Sec. Biomater. Bio-Inspired Mater. 9 (2022) 990931, https://doi.org/10.3389/fmats.2022.990931.

[6] X. Liu, Y. Zhang, Y. Wang, W. Zhu, G. Li, X. Ma, Y. Zhang, S. Chen, S. Tiwari, K. Shi, S. Zhang, H.M. Fan, Y.X. Zhao, X.J. Liang, Comprehensive understanding of magnetic hyperthermia for improving antitumor therapeutic efficacy, Theranostics 10 (8) (2020) 3793–3815, https://doi.org/10.7150/thno.40805.

[7] M.J. Molaei, Magnetic hyperthermia in cancer therapy, mechanisms, and recent advances: a review, J. Biomater. Appl. 39 (1) (2024) 3–23, https://doi.org/10.1177/08853282241244707.

[8] D. Chang, M. Lim, J.A.C.M. Goos, R. Qiao, Y.Y. Ng, F.M. Mansfeld, M. Jackson, T. P. Davis, M. Kavallaris, Biologically targeted magnetic hyperthermia: potential and limitations, Front. Pharmacol. 9 (2018) 831, https://doi.org/10.3389/fphar.2018.00831.

[9] A. Cochis, M. Miola, O. Bretcanu, L. Rimondini, E. Vernè, Magnetic bioactive glass ceramics for bone healing and hyperthermic treatment of solid tumors, in: A. Tiwari, P.K. Iyer, V. Kumar, H. Swart (Eds.), Advanced Magnetic and Optical Materials, 2016, pp. 81–112.

[10] O. Bretcanu, M. Miola, C.L. Bianchi, I. Marangi, R. Carbone, I. Corazzari, M. Cannas, E. Verné, In vitro biocompatibility of a ferrimagnetic glass-ceramic for hyperthermia application, Mater. Sci. Eng., C 73 (2017) 778–787, https://doi.org/10.1016/j.msec.2016.12.105.

[11] M. Miola, Y. Pakzad, S. Banijamali, S. Kargozar, C. Vitale-Brovarone, A. Yazdanpanah, O. Bretcanu, A. Ramedani, E. Vernè, M. Mozafari, Glass-ceramics for cancer treatment: so close, or yet so far? Acta Biomater. 83 (2019) 55–70, https://doi.org/10.1016/j.actbio.2018.11.013.

[12] M.V. Velasco, M.T. Souza, Murilo C. Crovace, A.J. Aparecido de Oliveira, E. D. Zanotto, Bioactive magnetic glass-ceramics for cancer treatment, Biomed. Glasses 5 (1) (2019) 148–177, https://doi.org/10.1515/bglass-2019-0013.

[13] S.S. Danewalia, K. Singh, Bioactive glasses and glass–ceramics for hyperthermia treatment of cancer: state-of-art, challenges, and future perspectives, Mater. Today Bio 10 (2010) 100100, https://doi.org/10.1016/j.mtbio.2021.100100.

[14] M. Miola, Bioactive magnetic glass–ceramics for cancer treatment, in: S. Kargozar, M. Mozafari (Eds.), Biomaterials for Precision Cancer Medicine, Woodhead Publishing Series in Biomaterials, 2025, pp. 203–236, https://doi.org/10.1016/B978-0-323-85661-4.00002-0. Elsevier Science Ltd.

[15] S. Miwa, T. Shirai, N. Yamamoto, K. Hayashi, A. Takeuchi, K. Tada, Y. Kajino, H. Inatani, T. Higuchi, K. Abe, Y. Taniguchi, H. Tsuchiya, Risk factors for postoperative deep infection in bone tumors, PLoS One 12 (11) (2017) e0187438, https://doi.org/10.1371/journal.pone.0187438.

[16] S. Miwa, N. Yamamoto, K. Hayashi, A. Takeuchi, K. Igarashi, H. Tsuchiya, Surgical site infection after bone tumor surgery: risk factors and new preventive techniques, Cancers (Basel) 14 (18) (2022) 4527, https://doi.org/10.3390/cancers14184527.

[17] I. Unalan, I. Occhipinti, M. Miola, E. Vernè, A.R. Boccaccini, Development of superparamagnetic iron oxide nanoparticle-coated melt electrowritten scaffolds for biomedical applications, Macromol. Biosci. 24 (2024) 2300397, https://doi.org/10.1002/mabi.202300397.

[18] A. Hlukhaniuk, M. Świętek, V. Patsula, O. Janoušková, A. Brož, M. Malić, A. Kołodziej, A. Wesełucha-Birczyńska, J. Hodan, M. Slouf, W. Tokarz, B. Zasońska, L. Bystrianský, M. Gryndler, L. Bačáková, D. Horák, Electrospun PCL mats modified with magnetic nanoparticles and tannic acid with antibacterial and possible antiosteosarcoma activity for bone tissue engineering and cancer treatment, ACS Biomater. Sci. Eng. 11 (7) (2025) 4315–4330, https://doi.org/10.1021/acsbiomaterials.5c00116.

[19] E. Vernè, M. Miola, S. Ferraris, C.L. Bianchi, A. Naldoni, G. Maina, O. Bretcanu, Surface activation of a ferrimagnetic glass–ceramic for antineoplastic drugs grafting, Adv. Eng. Mater. 12 (2010) B309–B319. https://hdl.handle.net/2434/147384.

[20] E.D. Teodor, F. Gatea, A. Ficai, G.L. Radu, Functionalized magnetic nanostructures for anticancer therapy, Curr. Drug Targets 19 (3) (2018) 239–247, https://doi.org/10.2174/1389450117666160208145835. Feb.

[21] C. Wu, W. Fan, Y. Zhu, M. Gelinsky, J. Chang, G. Cuniberti, V. Albrecht, T. Friis, Y. Xiao, Multifunctional magnetic mesoporous bioactive glass scaffolds with a hierarchical pore structure, Acta Biomater. 7 (2011) 3563–3572, https://doi.org/10.1016/j.actbio.2011.06.028.

[22] S. Shirgill, G. Poologasundarampillai, S. Jabbari, J. Ward, S.A. Kuehne, Silver-doped bioactive glass fibres as a potential treatment for wound-associated bacterial biofilms, Biofilm 5 (2023) 100115, https://doi.org/10.1016/j.bioflm.2023.100115.

[23] J. Barberi, L. Mandrile, A.M. Giovannozzi, M. Miola, L. Napione, A.M. Rossi, A. Vitale, S. Yamaguchi, S.- Spriano, Effect on albumin and fibronectin adsorption of silver doping via ionic exchange of a silica-based bioactive glass, Ceram. Int. 49 (9) (2023) 13728–13741, https://doi.org/10.1016/j.ceramint.2022.12.251.

[24] M. Lallukka, A. Houaoui, M. Miola, S. Miettinen, J. Massera, E. Verné, In vitro cytocompatibility of antibacterial silver and copper-doped bioactive glasses, Ceram. Int. 49 (22) (2023) 36044–36055, https://doi.org/10.1016/j.ceramint.2023.08.284.

[25] A. Prasad, V. Sowjanya, Jerold Manuel, P. Venkateswara Rao, Narayanan Madaboosi, P. Syam Prasad, Silver-doped bioactive spherical glass ceramic nanoparticles with enhanced osteogenic and antibacterial properties for bone tissue engineering, Colloids Surf. A Physicochem. Eng. Asp. 730 (2026) 139019, https://doi.org/10.1016/j.colsurfa.2025.139019.

[26] E. Vernè, S. Di Nunzio, M. Bosetti, P. Appendino, C. Vitale Brovarone, G. Maina, M. Cannas, Surface characterization of silver-doped bioactive glass, Biomaterials 26 (2005) 5111–5119, https://doi.org/10.1016/j.biomaterials.2005.01.038.

[27] M. Belay Taye, H. Setia Ningsih, S.J. Shih, Antibacterial and in vitro bioactivity studies of silver-doped, cerium-doped, and silver–cerium Co-Doped 80S mesoporous bioactive glass particles via spray pyrolysis, Appl. Sci. 13 (2023) 12637, https://doi.org/10.3390/app132312637.

[28] K. Sharma, Sher Singh Meena, Sudhanshu Saxena, S.M. Yusuf, A. Srinivasan, G. P. Kothiyal, Structural and magnetic properties of glass-ceramics containing silver and iron oxide, Mater. Chem. Phys. 133 (2012) 144–150, https://doi.org/10.1016/j.matchemphys.2011.12.085.

[29] M. Miola, R. Gerbaldo, F. Laviano, M. Bruno, E. Vernè, Multifunctional ferrimagnetic glass–ceramic for the treatment of bone tumor and associated complications, J. Mater. Sci. 52 (2017) 9192–9201, https://doi.org/10.1007/s10853-017-1078-6.

[30] M. Miola, M. Bruno, R. Gerbaldo, F. Laviano, E. Vernè, Melt-derived copper-doped ferrimagnetic glass-ceramic for tumor treatment, International 47 (2021) 31749–31755, https://doi.org/10.1016/j.ceramint.2021.08.056.

[31] M. Miola, M. Bruno, E. Vernè, Ferrimagnetic devitrified glass doped with copper by ion exchange: microstructure, bioactivity and antibacterial properties, Ceram. Int. 50 (2024) 12737–12745, https://doi.org/10.1016/j.ceramint.2024.01.178.

[32] O. Bretcanu, E. Vernè, M. Coisson, P. Tiberto, P. Allia, Magnetic properties of the ferrimagnetic glass-ceramics for hyperthermia, J. Magn. Magn Mater. 305 (16) (2006) 529–533, https://doi.org/10.1016/j.jmmm.2006.02.264.

[33] E. Vernè, M. Miola, S. Ferraris, C.L. Bianchi, A. Naldoni, G. Maina, O. Bretcanu, Surface activation of a ferrimagnetic glass-ceramic for antineoplastic drugs advanced, Biomaterials 12 (2010) B309–B319, https://doi.org/10.1002/adem.200980082.

[34] S. Di Nunzio, C. Vitale Brovarone, S. Spriano, D. Milanese, E. Verné, V. Bergo, G. Maina, P. Spinelli, Silver containing bioactive glasses prepared by molten salt ion-exchange, J. Eur. Ceram. Soc. 24 (2004) 2935–2942, https://doi.org/10.1016/j.jeurceramsoc.2003.11.010.

[35] T. Kokubo, H. Takadama, How useful is SBF in predicting in vivo bone bioactivity? Biomaterials 27 (2006) 2907–2915, https://doi.org/10.1016/j.biomaterials.2006.01.017.

[36] NCCLS, NCCLS: performance standards for antimicrobial disk susceptibility tests, in: Approved Standard, ninth ed., NCCLS, Villanova, PA, 2003, pp. M2–A9.

[37] M. Miola, E. Vernè, Bioactive and antibacterial glass powders doped with copper by ion-exchange in aqueous solutions, Materials 9 (2016) 405–421, https://doi.org/10.3390/ma9060405.

[38] https://web.mit.edu/2.813/www/readings/Ellingham_diagrams.pdf. (Accessed 15 December 2025).

[39] L.L. Hench, J.R. Jones, P. Sepulveda, Bioactive materials for tissue engineering scaffolds, in: J.M. Pollak, L.L. Hench, P. Kemp (Eds.), Future Strategies for Tissue and Organ Replacement, Word Scientific Pub.Co Inc, Singapore, 2002, pp. 3–24.

[40] A. Vulpoi, C. Gruian, E. Vanea, L. Baia, S. Simon, H.J. Steinhoff, G. Göller, V. Simon, Bioactivity and protein attachment onto bioactive glasses containing silver nanoparticles, J. Biomed. Mater. Res. 100A (2012) 1179–1186, https://doi.org/10.1002/jbm.a.34060.